Development of Bridge Column Longitudinal Reinforcement in Oversized Pile Shafts

Juan Murcia-Delso[1]; Yujia Liu[2]; and P. Benson Shing, M.ASCE[3]

Abstract: This paper presents an experimental investigation to determine the embedment length required for longitudinal reinforcement in a bridge column extending into an oversized pile shaft, and the amount of transverse reinforcement required for the pile shaft to prevent premature bar anchorage failure due to concrete splitting induced by bar slip. Four full-scale column–oversized pile assemblies were tested under quasi-static cyclic lateral loading. The test specimens had different embedment lengths for the column reinforcement, different amounts of transverse reinforcement in the piles, different sizes of longitudinal bars, ranging from No. 8 to No. 18 (25 to 57 mm) bars, and different column-to-pile diameter ratios. All column–pile assemblies behaved in a ductile manner with plastic deformation occurring near the base of the columns despite some cone-shaped fractures and tensile splitting cracks occurring in the top portion of the piles. The test results show that the embedment length for the column reinforcement can be significantly reduced as compared to that required in current design specifications. The study also shows that an engineered steel casing designed according to a formula proposed here can effectively confine the pile shaft and significantly reduce splitting cracks. **DOI: 10.1061/(ASCE)ST.1943-541X.0001591.**

Author keywords: Development length; Bridge column; Pile shaft; Reinforced concrete; Reinforcing bars; Large-scale testing; Concrete and Masonry Structures.

Introduction

Cast-in-drilled hole (CIDH) piles are frequently used as foundations of bridge columns because they have a smaller footprint than spread footings. When a column is extended into the soil with a pile of the same diameter, plastic deformation is expected to form in the pile below the ground surface when the column is subjected to severe lateral seismic forces, as depicted in Fig. 1. A properly designed pile with a cross section larger than that of the column it supports can shift plastic deformation to the base of the column. The latter system is, therefore, more convenient for postearthquake inspection and repair. However, because of the different cross sectional dimensions of the column and the pile, it is not possible to have a continuous reinforcement cage, and the column longitudinal reinforcement extended into the pile has to form a noncontact lap splice with the longitudinal reinforcement of the pile, as depicted in Fig. 1.

The *Seismic design criteria* (SDC) of the California Department of Transportation (Caltrans 2013) and the AASHTO *LRFD seismic bridge design specifications* (SBDS) (AASHTO 2011) require that column longitudinal reinforcement extended into an oversized pile shaft be terminated in a staggered manner with minimum embedment lengths of $D_{c,\max} + l_d$ and $D_{c,\max} + 2l_d$, respectively, where $D_{c,\max}$ is the larger cross-sectional dimension of the column and l_d is the required development length for a straight bar in tension determined according to Article 5.11.2.1 of the AASHTO *LRFD bridge design specifications* (BDS) (AASHTO 2010) using expected values of material properties. Such a requirement was determined to be very conservative based on the results of a study carried out by McLean and Smith (1997). Nevertheless, there were no experimental data available to arrive at an adequate recommendation for the embedment length, especially for large-diameter bars in large bridge columns, which can incur high construction costs. While a number of experiments have been conducted to study the development and lap-splice lengths of reinforcing bars, including noncontact lap splices subjected to cyclic loading (e.g., Lukose et al. 1982; Sagan et al. 1991), only McLean and Smith (1997) and Tran et al. (2013) have studied the development of column longitudinal reinforcement embedded in oversized pile shafts. Both studies used reduced-scale laboratory specimens. However, in the study of Tran et al. (2013), the columns were connected to the piles with headed bars, which is not the focus of this paper.

This paper presents the results of an experimental investigation to determine the minimum embedment length for column reinforcements extending into an oversized pile shaft, and the amount of transverse reinforcement required along the bar anchorage region of the pile shaft to prevent premature anchorage failure. In this investigation, four full-scale reinforced concrete bridge column–oversized pile assemblies were tested under quasi-static cyclic lateral loading. Based on data from companion studies reported elsewhere (Murcia-Delso et al. 2013a, 2015), it was decided that three of the assemblies had embedment lengths substantially shorter than those required in the Caltrans (2013) and AASHTO (2011) specifications. Formulas proposed to determine these shorter embedment lengths and the amount of transverse reinforcement used in the tested piles are presented and explained in this paper.

Embedment Length for Column Reinforcement in Oversized Pile Shafts

For longitudinal bars extending from large-diameter bridge columns into oversized pile shafts, the Caltrans SDC (Caltrans 2013)

[1]Senior Researcher, Tecnalia Research and Innovation, Parque Cientifico y Tecnologico de Bizkaia, C/ Geldo, Edificio 700, 48160 Derio, Spain (corresponding author). E-mail: juan.murcia@tecnalia.com

[2]Graduate Student Researcher, Dept. of Structural Engineering, Univ. of California, San Diego, 9500 Gilman Dr., MC0085, La Jolla, CA 92093-0085.

[3]Professor, Dept. of Structural Engineering, Univ. of California, San Diego, 9500 Gilman Dr., MC0085, La Jolla, CA 92093-0085.

Note. This manuscript was submitted on October 7, 2015; approved on April 15, 2016; published online on June 27, 2016. Discussion period open until November 27, 2016; separate discussions must be submitted for individual papers. This paper is part of the ***Journal of Structural Engineering***, © ASCE, ISSN 0733-9445.

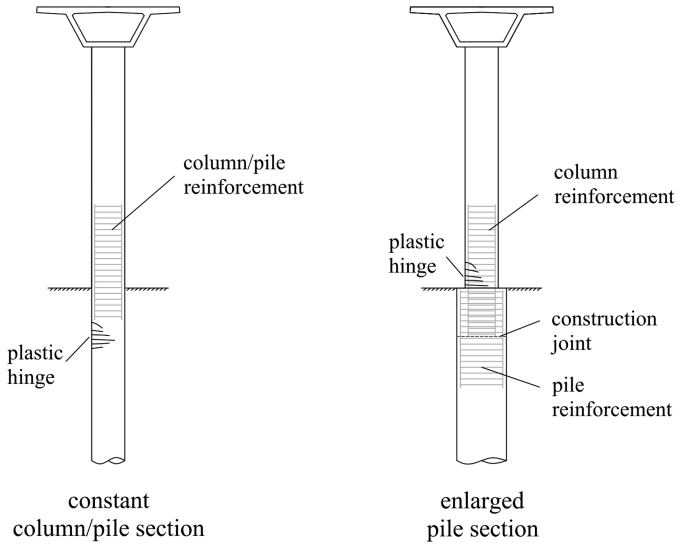

Fig. 1. Types of pile shafts

and the AASHTO LRFD SBDS (AASHTO 2011) requirements can result in embedment lengths significantly longer than the tension development length l_d specified in the AASHTO LRFD BDS (AASHTO 2010) because of the additional length $D_{c,\max}$, which is intended to account for damage that could spread into the bar anchorage zone of a pile shaft when plastic deformation develops at the column base.

The study by McLean and Smith (1997) has shown that noncontact lap splices in oversized pile shafts can perform satisfactorily with a lap length equal to $l_s + s$, where $l_s = 1.7 \times l_d$ is the lap length specified for Class C tension lap splices in the AASHTO LRFD BDS (AASHTO 2010), and s is the bar spacing in the noncontact lap splice. This lap length was determined by McLean and Smith (1997) based on a truss model, in which the forces between spliced bars are transferred through 45-degree-angle compression struts. They assumed that no strut action could form along a distance s from the top of the pile and validated the proposed lap length with tests on reduced-scale column-pile specimens that had No. 4 and 8 (12 and 25 mm) reinforcing bars. However, the applicability of the proposed lap length to large-size columns and large-diameter bars had not been verified, and whether the proposed lap length could be further reduced had not been investigated.

Murcia-Delso et al. (2015) conducted pull-push tests on individual large-diameter [No. 14 and 18 (43 and 57 mm)] bars anchored in cylindrical concrete specimens with reinforcement details similar to those in an enlarged pile shaft. Data from those tests and a numerical study using nonlinear finite-element models presented in Murcia-Delso et al. (2013a) have suggested that the embedment length, l_e, of the column longitudinal reinforcement inside the pile can be further reduced to that given in Eq. (1)

$$l_e = l_d + s + c \tag{1}$$

in which c = thickness of the concrete cover above the pile reinforcement; and l_d = tension development length specified in the AASHTO LRFD BDS (AASHTO 2010). The term $s + c$ in Eq. (1) accounts for the ineffective force transfer region in the upper part of the noncontact lap splice hypothesized by McLean and Smith (1997). The large-scale test results reported herein confirm the feasibility of using this reduced embedment length.

Transverse Reinforcement in the Bar Anchorage Region of Pile Shafts

It is crucial to have sufficient transverse reinforcement in the bar anchorage region of a pile shaft to prevent bond failures caused by concrete splitting and ensure adequate development of the column longitudinal bars (McLean and Smith 1997). Based on their truss model, McLean and Smith (1997) proposed Eq. (2) to calculate the maximum permissible spacing, $s_{tr,\max}$, of the transverse reinforcement to resist the strut force

$$s_{tr,\max} = \frac{2\pi A_{tr} f_{y,tr} l_s}{A_l f_u} \tag{2}$$

in which A_l and f_u = total cross-sectional area and tensile strength of the longitudinal reinforcement, respectively; A_{tr} and $f_{y,tr}$ = cross-sectional area and yield strength of the transverse hoops or spiral, respectively; and $l_s = 1.7 \times l_d$. Prior to 2012, the AASHTO LRFD BDS did not have specific provisions for transverse reinforcement in the bar anchorage region of an oversized pile shafts. In the 2012 Edition of the specifications (AASHTO 2012), Eq. (3) was introduced as a provision to determine the maximum permissible transverse reinforcement spacing

$$s_{tr,\max} = \frac{2\pi A_{tr} f_{y,tr} l_s}{k A_l f_{u,\min}} \tag{3}$$

in which $f_{u,\min}$ = minimum tensile strength of the column longitudinal reinforcement [which can be taken to be 550 MPa (80 ksi) for ASTM A706 steel (ASTM 2009)]; and k = ratio of the amount of column reinforcement that is in tension at the nominal moment capacity of the column to the total amount of column reinforcement. The value of k can be determined from a moment-curvature analysis; however, it can be assumed 0.5 for most applications (AASHTO 2012). Eq. (3) is similar to Eq. (2) except that the former, in most cases, results in greater spacing (i.e., significantly less transverse reinforcement) because the value of k will typically be less than 1.0.

The transverse reinforcement spacing calculated with either Eq. (2) or Eq. (3) is directly proportional to the lap length l_s, determined with the formula proposed by McLean and Smith (1997). Eq. (2) was developed with the assumption that the diagonal strut force and thereby the bond stress distribution along the effective lap length were uniform and inversely proportional to the lap length. That assumption does not account for higher-than-average local bond-stress demand and associated radial stress induced in the surrounding concrete by the bar slip. New formulas, which avoid that assumption, have been proposed in this study to determine the minimum amount of transverse reinforcement required to prevent premature bond failure caused by concrete splitting in the bar anchorage region of the pile. More stringent formulas have also been proposed to control the width of splitting cracks. The derivation of the formulas is shown in the Appendix.

The new formulas used to design the test specimens are presented in Eqs. (4) and (5). Eq. (4) determines the maximum permissible transverse reinforcement spacing to prevent bond failure due to concrete splitting as follows:

$$s_{tr,\max} = \frac{2\pi A_{tr} f_{y,tr}}{N_{\text{col}} d_{b,\text{col}} \tau_{\max}} \tag{4}$$

in which N_{col} = number of longitudinal bars in the column; $d_{b,\text{col}}$ = diameter of the column longitudinal bars; and $\tau_{\max}$ = maximum bond strength of the bars. The value of $\tau_{\max}$ can be taken to be 16.5 MPa (2.4 ksi) for 34.5 MPa (5 ksi) concrete based on the bond-slip tests conducted by Murcia-Delso et al. (2013b) on bars with similar confinement conditions as those in an oversized pile

shaft. For concrete strengths other than 34.5 MPa (5 ksi), $\tau_{\max}$ can be assumed to be proportional to $f_c'^{3/4}$ (Murcia-Delso et al. 2013b).

Eq. (5) is for determining the wall thickness $t_{c,\min}$ of an engineered steel casing that can be used to control the width of tensile splitting cracks in the pile. The use of an engineered steel casing around a pile can serve the same purpose as the transverse reinforcement and avoid unreasonably close spacing of the transverse hoops. It also retains the soil around the drilled hole and provides a safer environment for construction

$$t_{c,\min} = \frac{1}{\alpha_2 f_{y,c}} \left(\frac{1}{2\pi} N_{\text{col}} \tau_{\max} d_{b,\text{col}} - \alpha_1 \frac{A_{tr}}{s_{tr}} f_{y,tr} \right) \tag{5a}$$

In Eq. (5a), $u_{cr,\max}$ = maximum allowed nominal width of the radial splitting cracks in the pile; $f_{y,c}$ = nominal yield strength of the casing steel; s_{tr} = spacing of the pile transverse reinforcement; and α_1 and α_2 are calculated with Eqs. (5b) and (5c), respectively

$$\alpha_1 = \frac{u_{cr,\max} N_{sh}}{\pi D_{\text{ext}} \varepsilon_{y,tr}} \leq 1 \tag{5b}$$

$$\alpha_2 = \frac{u_{cr,\max} N_{sh}}{\pi D_s \varepsilon_{y,c}} \leq 1 \tag{5c}$$

in which N_{sh} = number of pile longitudinal bars; D_{ext} = diameter of the pile transverse hoops (or spiral); $\varepsilon_{y,tr}$ = yield strain of the transverse hoops; D_s = diameter of the steel casing; and $\varepsilon_{y,c}$ = yield strain of the casing steel.

Test Specimens

Four column–pile assemblies were tested. Three of them had embedment lengths conforming to Eq. (1), and two of the three specimens had transverse reinforcement satisfying Eqs. (4) and (5), respectively. Each test specimen consisted of a bridge column and the upper portion of a pile shaft. The top of the column was subjected to fully reversed cyclic lateral displacements and the base of the pile segment was fixed to the strong floor in the laboratory, as shown in Fig. 2. The height of the pile segment, H_p, was so determined that the base of the segment would more or less correspond to the section where the maximum moment would have developed in the full-length pile (Liu 2012). However, due to the absence of soil, the maximum moment demand at the base of the pile segment would be slightly higher than that in the actual pile.

The geometries and reinforcing details of the test specimens are summarized in Table 1. All specimens had a 1,219-mm (4-ft) diameter column, and the height-to-diameter ratios of the columns varied from 4 to 4.5. The piles in Specimens 1 through 3 had a diameter of 1,829 mm (6 ft), while Specimen 4 had a 1,524-mm (5-ft) diameter pile. The height-to-diameter ratios of the piles were between 1.2 and 1.5. The design of the piles satisfies Section 7.7.3.2 of the Caltrans SDC (Caltrans 2013), which requires that the ratio of the expected nominal moment capacity of a pile shaft to the moment demand generated by the over-strength moment at the base of the column be no less than 1.25 at any section. The maximum value of this ratio, occurring at the base of the pile segment, was calculated to be 1.67 for Specimen 1, 1.98 for Specimens 2 and 3, and 1.26 for Specimen 4. The size of the longitudinal reinforcing bars in the columns varied from No. 8 to No. 14 (25 to 43 mm), and that in the piles from No. 11 to No. 18 (36 to 57 mm). Columns in Specimens 1 and 4 had less longitudinal reinforcement than Specimens 2 and 3.

The design of the column and the pile in Specimen 1 complied with the Caltrans BDS (Caltrans 2008) and Caltrans SDC (Caltrans 2013), with the exception of the embedment length of the column reinforcement inside the pile. The embedment length was $D_{c,\max} + l_d$, in which l_d was determined in accordance with the AASHTO LRFD BDS (AASHTO 2010) and AASHTO LRFD SBDS (AASHTO 2011). The requirement to terminate half of the longitudinal bars at $D_{c,\max} + 2l_d$ was not followed. This reduction in embedment length was proved to be safe by a pretest finite-element analysis of the column–pile assembly (Murcia-Delso et al. 2013a). The transverse reinforcement in the entire pile segment was determined according to the design requirements for compression members in Article 5.7.4.6 of the AASHTO LRFD BDS (AASHTO 2010).

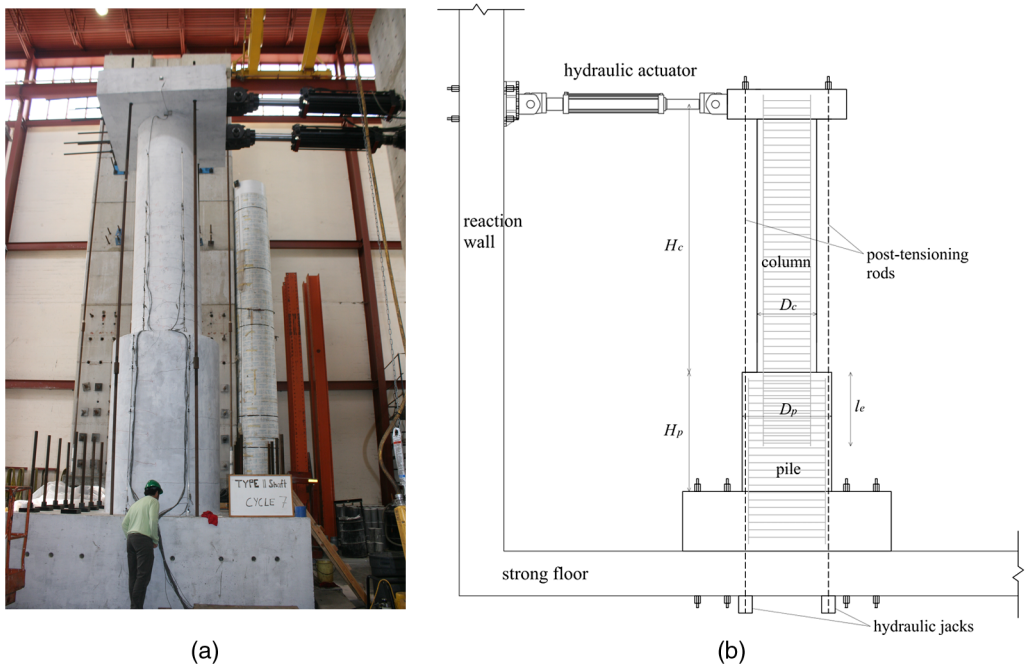

Fig. 2. Tests on column-oversized pile assemblies: (a) test specimen; (b) test specimen geometry and setup

Table 1. Dimensions and Reinforcing Details of Test Specimens

Design parameter	Specimen 1	Specimen 2	Specimen 3	Specimen 4
Column diameter, D_c [mm (ft)]	1,219 (4)	1,219 (4)	1,219 (4)	1,219 (4)
Pile diameter, D_p [mm (ft)]	1,829 (6)	1,829 (6)	1,829 (6)	1,524 (5)
Column height[a], H_c [mm (ft)]	4,877 (16)	5,486 (18)	5,486 (18)	4,877 (16)
Pile height, H_p [mm (ft)]	2,743 (9)	2,439 (8)	2,439 (8)	1,829 (6)
Column longitudinal steel (reinforcement ratio)	18 No. 11 (1.55%)	18 No. 14 (2.24%)	18 No. 14 (2.24%)	32 No. 8 (1.40%)
Pile longitudinal steel (reinforcement ratio)	28 No. 14 (1.55%)	26 No. 18 (2.55%)	26 No. 18 (2.55%)	40 No. 11 (2.21%)
Formula for embedment length of column reinforcement	$D_{c,\max} + l_d$	$l_d + s + c$	$l_d + s + c$	$l_d + s + c$
Embedment length of column reinforcement [mm (ft)]	2,286 (7.5)	1,829 (6)	1,829 (6)	940 (3.08)
Formula for transverse steel in bar anchorage region of pile	Compression Member—AASHTO (2010)	Eq. (2)—McLean and Smith (1997)	Eq. (5)	Eq. (4)
Transverse pile steel in bar anchorage region of pile (volumetric ratio)	Two No. 6 at 165 mm (6.5 in.) (0.82%)	Two No. 7 at 178 mm (7 in.) (1.04%)	No. 8 at 165 mm (6.5 in.), and 6.3-mm (0.25-in.) steel casing (1.65%[b])	Two No. 7 at 140 mm (5.5 in.) (1.62%)
Transverse steel in plastic-hinge region of column (volumetric ratio)	Two No. 5 at 165 mm (6.5 in.) (0.87%)	Two No. 5 at 102 mm (4 in.) (1.41%)	Two No. 5 at 102 mm (4 in.) (1.41%)	No. 6 at 102 mm (4 in.) (1.0%)

Note: No. 5 = 16 mm, No. 6 = 19 mm, No. 7 = 22 mm, No. 8 = 25 mm, No. 11 = 36 mm, No. 14 = 43 mm, No. 18 = 57 mm.
[a]Height from the column base to the point of the horizontal load application.
[b]Based on equivalent amount of Grade 60 transverse steel.

Specimens 2 through 4 were designed according to the current practice by Caltrans, which follows the AASHTO LRFD BDS (AASHTO 2010) and the Caltrans SDC (Caltrans 2013), with the exception of the embedment length of the column reinforcement inside the pile, which was reduced to $l_d + s + c$. Another exception was the amount of the transverse reinforcement in the bar anchorage region of the piles. For Specimen 2, the amount of the transverse reinforcement was determined with Eq. (2) but with l_d replacing l_s to be consistent with the actual embedment length used. The amount of the transverse reinforcement in the bar anchorage region of Specimens 3 and 4 was determined with Eqs. (5) and (4), respectively. Specimen 3 was identical to Specimen 2, except that the horizontal hoop reinforcement in the pile was reduced to the minimum required for compression members as defined in Article 5.7.4.6 of the AASHTO LRFD BDS (AASHTO 2010), and a permanent engineered steel casing was added around the entire height of the pile to provide adequate confinement to control the width of the tensile splitting cracks. The steel casing was 6.4 mm (0.25 in.) thick and was made of A36 steel. It had a 24.5-mm (1-in.) gap from the base slab of the specimen. The thickness of the steel casing was determined with Eq. (5) using the maximum allowable crack width $u_{cr,\max}$ of 0.3 mm (0.012 in.) recommended by the American Concrete Institute (ACI 2001) for RC members in contact with soil under service conditions. Specimen 4 had a pile diameter only 305 mm (1 ft) larger than that of the column, which did not meet the requirement that the cross-sectional dimension of an oversized pile be at least 610 mm (2 ft) larger than that of the column (Caltrans 2013). However, the pile-to-column diameter ratio for the specimen corresponds to that of an 2438 mm (8 ft)-diameter column supported on a 3048 mm (10 ft)-diameter pile, which meet the previously mentioned Caltrans requirement. The amount of the transverse reinforcement in the bar anchorage region of Specimen 4 was the minimum required to prevent bar anchorage failure, as determined by Eq. (4).

Material Properties and Instrumentation

The concrete for the piles and columns had a specified compressive strength of 31 MPa (4,500 psi) at 28 days, a slump of 178 mm (7 in.) and 102 mm (4 in.), respectively, and a maximum aggregate size of 9.5 mm (3/8 in.) and 25 mm (1 in.), respectively. The column–pile assemblies were tested when the concrete strengths in the column and the pile were close to 34.5 MPa (5,000 psi). The actual strengths of the concrete on the days of the tests are presented in Table 2. The reinforcing steel was Grade 60 complying with the ASTM A706 standards. Results from material tests on steel samples are also presented in Table 2. The yield and tensile strengths of the A36 steel used for the pile casing for Specimen 3 were 324 MPa (47.0 ksi) and 472 MPa (68.4 ksi), respectively.

The strains in the longitudinal and transverse reinforcement in the piles and the columns were measured with electrical resistance strain gauges. Fig. 3 shows the locations of the strain gauges in Specimen 1, which were installed at different elevations. In the plastic hinge region of the column and the bar anchorage region of the pile, strain gauges were installed at 305 mm (1 ft) spacing in the longitudinal bars and at every other transverse hoop. Similar strain gauge locations were used in the other specimens. Strain gauges were also installed to measure hoop strains in the steel casing of Specimen 3. Displacement transducers were mounted to measure the lateral displacement of the column–pile assemblies and to provide data to calculate flexural and shear deformations as well as rotation at the base of the columns. Detailed instrumentation plans for the test specimens are provided in Murcia-Delso et al. (2013a).

Loading Protocol

The top of the column was subjected to a constant vertical load of 3,559 kN (800 kips) during the entire test. Together with the self-weight of the specimen, this load subjected the base of the column to an axial stress equal to 9.4% of the target compressive strength of the concrete, which was 34.5 MPa (5,000 psi). It represented the axial load carried by a typical bridge column. The vertical load was applied with four posttensioning rods. Anchored at the top face of the column head, these rods passed through holes in the column head, the footing, and the strong floor, and were subjected to a constant force using four center-hole hydraulic jacks located beneath the strong floor, as shown in Fig. 2(b). The pressure in the jacks was regulated to keep the force constant as the top of the column was

Table 2. Strengths of Concrete and Longitudinal Steel

Specimen number	Region	Compressive strength of concrete [MPa (ksi)]	Longitudinal bar size	Yield strength [MPa (ksi)]	Tensile strength [MPa (ksi)]
Specimen 1	Pile anchorage region	34.5 (5.0)	No. 14 (43 mm)	484 (70.1)	672 (97.4)
	Pile below anchorage region	42.8 (6.2)			
	Column lower 2.8 m (9 ft)	34.0 (4.9)	No. 11 (36 mm)	448 (65.0)	629 (91.2)
	Column upper 2.1 m (7 ft)	38.6 (5.6)			
Specimen 2	Pile anchorage region	37.0 (5.4)	No. 18 (57 mm)	462 (67.0)	641 (93.0)
	Pile below anchorage region	39.7 (5.8)			
	Column lower 2.8 m (9 ft)	38.6 (5.6)	No. 14 (43 mm)	462 (67.0)	638 (92.5)
	Column -upper 2.4 m (8 ft)	40.7 (5.9)			
Specimen 3	Pile anchorage region	36.2 (5.3)	No. 18 (57 mm)	462 (67.0)	652 (94.5)
	Pile below anchorage region	34.1 (4.9)			
	Column lower 2.8 m (9 ft)	35.0 (5.1)	No. 14 (43 mm)	462 (67.0)	641 (93.0)
	Column upper 2.4 m (8 ft)	33.2 (4.8)			
Specimen 4	Pile anchorage region	36.6 (5.3)	No. 11 (36 mm)	445 (64.5)	634 (92.0)
	Pile below anchorage region	33.0 (4.8)			
	Column lower 2.8 m (9 ft)	35.5 (5.1)	No. 8 (25 mm)	459 (66.5)	650 (94.3)
	Column upper 2.1 m (7 ft)	33.9 (4.9)			

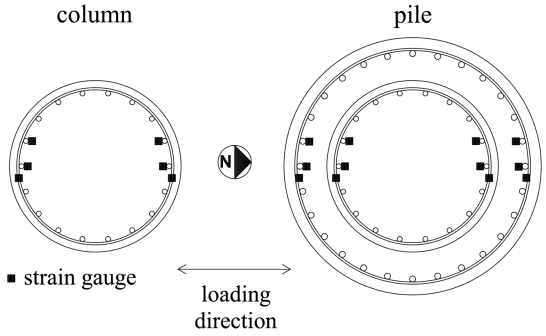

Fig. 3. Location of strain gauges in Specimen 1

displaced laterally in the north–south direction using two 979-kN (220-kip) capacity, 1,219-mm (48-in.) stroke, servo-controlled hydraulic actuators. The loading protocol used is shown in Fig. 4. Initially, each specimen was subjected to four fully-reversed force-controlled lateral load cycles, with amplitudes equal to 25, 50, 75, and 100% of the predicted load, F_y', defined herein as the load that would cause the longitudinal reinforcement in the column to reach the first yield. The specimen was then subjected to fully reversed displacement-controlled load cycles with increasing ductility demands of 1, 2, 3, and higher until the lateral load resistance dropped significantly due to the fracture of the longitudinal bars in the column. Each ductility level had two load cycles. The ductility demand was defined as $\mu = \Delta/\Delta_y$, in which Δ was the lateral displacement of the specimen at the elevation of the horizontal actuators and Δ_y was the effective yield displacement. As shown in Fig. 4(a), Δ_y was defined as the displacement at the intersection of the secant line through the zero-load point and (Δ_y', F_y') with a horizontal line representing the theoretical ultimate resistance (F_y), which was defined as the effective yield force. To define the loading protocol, F_y' and F_y were determined by finite-element analyses, and the value of Δ_y' was obtained as the average of the absolute maximum displacements measured in the two opposite loading directions in Cycle 4 of the test.

Load-versus-Displacement Relations

The measured lateral load-versus-drift relations are shown in Fig. 5. The drift was measured at the top of the column where the horizontal load was applied. The loading and displacement are defined herein as positive when they are towards the south. As shown in Fig. 5, all four column–pile assemblies had a ductile behavior, exhibiting a mild drop of lateral resistance as the column displacement increased until a large drift level was reached. The gradual load decrease was caused by the $P-\Delta$ effect of the vertical force. The tests were stopped when the lateral load capacity started to drop significantly due to low-cycle fatigue fracture of one or more longitudinal bars at the base of the column. Bar fracture occurred when

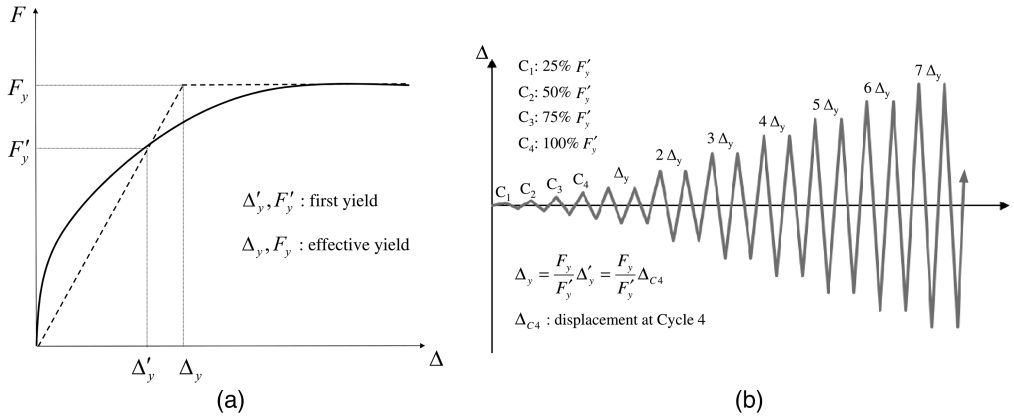

Fig. 4. Loading protocol: (a) first yield and effective yield point; (b) loading history

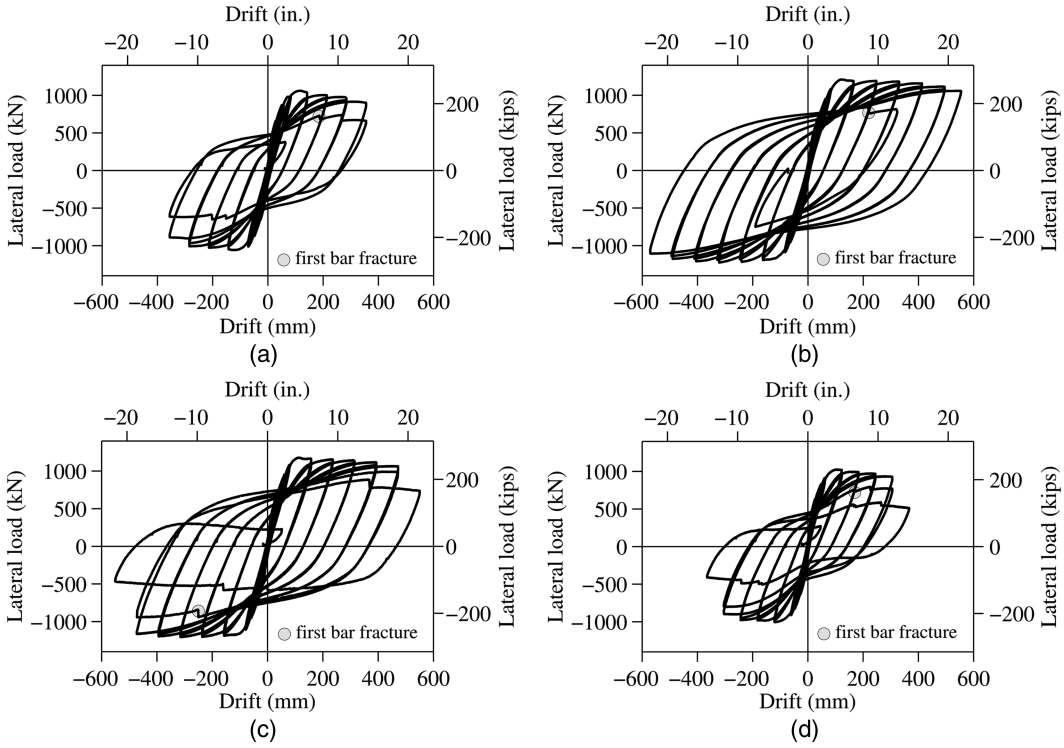

Fig. 5. Lateral force versus drift curves: (a) Specimen 1; (b) Specimen 2; (c) Specimen 3; (d) Specimen 4

Table 3. Load and Displacement Capacities

Specimen number	Maximum lateral load [kN (kip)]	Equivalent yield displacement (Δ_y) [mm (in.)]	Displacement ductility capacity[a]
Specimen 1	1,063 (239)	64 (2.5)	5.5
Specimen 2	1,223 (275)	83 (3.3)	6.9
Specimen 3	1,205 (271)	79 (3.1)	6.3
Specimen 4	1,023 (230)	56 (2.2)	5.5

[a]Maximum ductility attained prior to the fracture of a column longitudinal bar.

a severely buckled bar was subjected to tension again upon load reversal. The maximum lateral load resistances, effective yield displacements, and displacement ductility capacities of the test specimens are summarized in Table 3. The effective yield displacement Δ_y and ductility μ are defined in the same way as those used to determine the loading protocol except that they are based on the actual maximum load and actual first yield attained in the tests. The ductility capacity of a specimen is determined as the maximum ductility attained prior to the fracture of a longitudinal bar. The ductility capacities attained are between 5.5 (for Specimens 1 and 4) and 6.9 (for Specimen 2).

The test results show that the size of the longitudinal reinforcing bars and the spacing of the transverse reinforcement in the columns had a noticeable influence on the ductility capacity of the columns. Columns with smaller bars (Specimen 4) or larger spacing of transverse hoops (Specimen 1) had earlier bar buckling and fracture and were, therefore, less ductile. This consistent with Euler's buckling theory that the more slender the bar is, the lower its buckling resistance will be. The drift at which a longitudinal bar in the plastic-hinge region of the column would fracture was also slightly affected by the confinement level in the bar anchorage region of the pile. The pile in Specimen 3 had a better confinement, due to the steel casing, than Specimen 2. The better confinement resulted in a higher bond resistance developing in the column longitudinal bars anchored in the pile, and therefore less bar slip, less plastic strain penetration into the pile, and more severe plastic strains in the plastic-hinge region of the column, leading to slightly earlier bar fracture. Consequently, Specimen 3 had slightly lower ductility than Specimen 2.

General Test Observations

Pictures of the damaged specimens are shown in Figs. 6–10. The specimens showed similar damage progressions. In every specimen, prior to the yielding of the column longitudinal bars, flexural cracks formed in the column and in the pile. After some of the longitudinal bars had yielded at the base of the column, crushing of concrete was observed in the compression toes. In subsequent cycles, gradual spalling of the concrete cover was observed near the base of the column. Fig. 6 presents the progression of damage near the base of the column in Specimen 1. Some of the column longitudinal bars in this specimen started to buckle during the first cycle at $\mu = 5.5$. The severely buckled bars fractured when they were subjected to tension again upon load reversal. For Specimen 2, only one bar fractured during the second cycle at $\mu = 6.9$ owing to the closer spacing of the transverse hoops at the base of the column, which delayed bar buckling. Specimen 3, which had column reinforcement identical to that in Specimen 2, had column bar fracture in the first cycle at $\mu = 6.3$. Specimen 4 had column bar fracture in the first cycle at $\mu = 5.5$. The earlier bar fracture in this specimen can be attributed to the smaller bar size while the hoop spacing remained the same as that in Specimens 2 and 3, which made the bars more vulnerable to buckling, as explained in the previous section.

Fig. 7 shows the damage in the pile of Specimen 1. Several radial cracks extended horizontally from the column base to the edge of

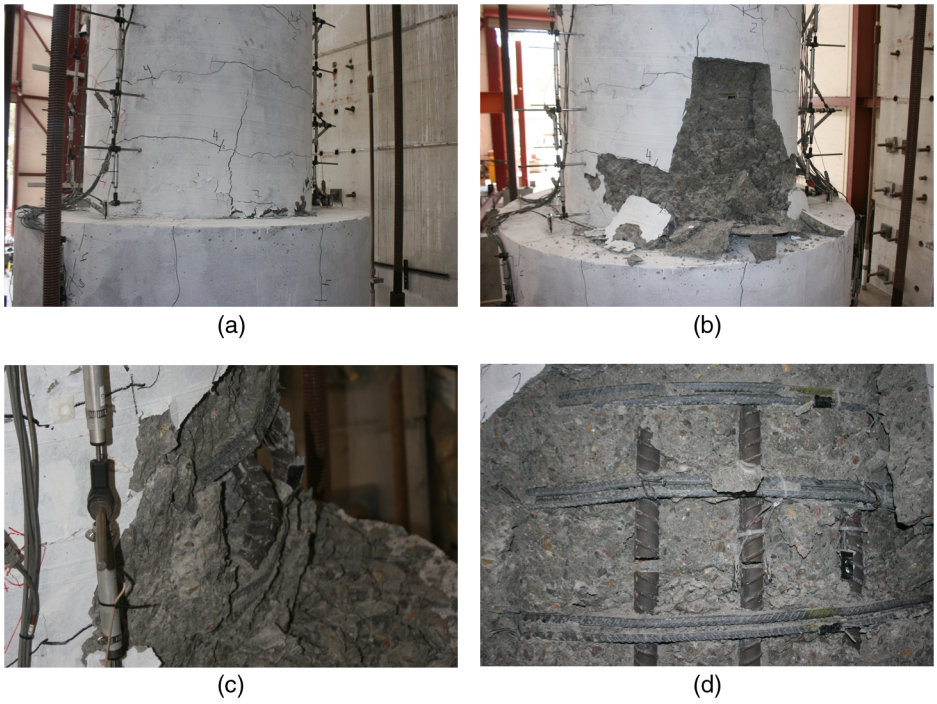

Fig. 6. Evolution of damage near the column base of Specimen 1: (a) $\mu = 2.2$; (b) $\mu = 4.4$; (c) $\mu = 5.5$ (first cycle); (d) $\mu = 5.5$ (second cycle)

Fig. 7. Damage in the pile of Specimen 1: (a) circular and splitting cracks; (b) lengths of splitting cracks

the pile. They were the result of splitting forces generated by bar slip. The maximum residual width measured in one of the cracks at the end of the test was approximately 3 mm (1/8 in.). The splitting cracks extended vertically on the lateral surface of the pile with lengths ranging from 600 mm (2 ft) to 1,200 mm (4 ft), which corresponds to the upper 25 to 50% of the embedment length of the column reinforcement. The pile of Specimen 2 was more severely damaged than that of Specimen 1, as shown in Fig. 8. In the first cycle at $\mu = 5$, the maximum width of the splitting cracks measured after unloading was 6 mm (1/4 in.), twice as wide as that in Specimen 1. In addition, more splitting cracks were observed, which extended vertically on the lateral surface of the pile with lengths ranging from 900 mm (3 ft) to 1,200 mm (4 ft), which corresponds to 50 to 66% of the embedment length of the column reinforcement. The more-severe damage observed in the pile of Specimen 2 can be explained by the larger splitting forces generated by the larger diameter bars [as observed in the development length tests of Murcia-Delso et al. (2015)], the higher ductility of the column (imposing more-severe demands on the pile), and also the shorter embedment length of the column longitudinal bars (leading to more-severe bar slip). At the end of the test of Specimen 2, the cracks on the top of the pile opened so widely that pieces of concrete could be removed by hand. Fig. 8(c) shows a picture taken after these pieces were removed. A cone-shaped fracture surface with a slope of approximately 25 degrees formed between the column and the pile steel cages, and radial splitting cracks at the location of the longitudinal bars in the column and the pile were visible.

The pile of Specimen 3 experienced very minor damage, as shown in Fig. 9. The steel casing was effective in restraining the opening of the splitting cracks and protecting the pile from severe cracking. The maximum residual width of the radial splitting cracks observed after unloading in the first cycle at $\mu = 5.2$ was approximately 0.3 mm (0.012 in.), which is significantly smaller than that in Specimen 2 after experiencing the same ductility demand. The maximum residual width of the splitting cracks observed after the test was 1 mm (0.04 in.) and a much shallower cone-shaped facture surface was observed on the top of the pile. After the test, the steel casing was removed revealing almost no damage in the pile, as

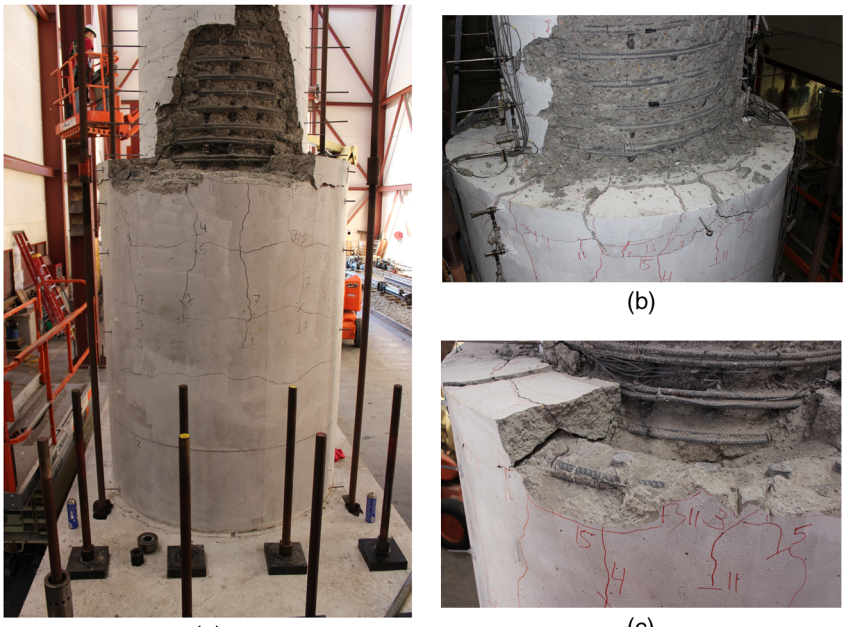

Fig. 8. Damage in Specimen 2: (a) column base and pile; (b) cracks atop of the pile; (c) fracture surface atop of the pile

Fig. 9. Damage in Specimen 3: (a) column base and top of the pile; (b) pile after removal of the steel casing

Fig. 10. Cracks atop of the pile of Specimen 4

shown in Fig. 9(b). Splitting cracks extended vertically less than 305 mm (1 ft) from the top of the pile, and their maximum width was approximately 0.2 mm (0.008 in.) occurring at just a few inches below the top of the pile. The pile of Specimen 4 had severe splitting cracks, as shown in Fig. 10. In the first cycle at $\mu = 5.5$, some of the splitting cracks opened widely at the top of the pile [with a maximum residual crack width of approximately 10 mm (0.4 in.) after unloading] and had propagated along the entire embedment length of the column reinforcement. At the end of the test, the maximum residual width of the splitting cracks was larger than 15 mm (0.6 in.). In addition, a circular crack was observed around the column reinforcement cage, indicating the formation of a small cone-shaped breakoff.

Curvatures along the Specimens

Fig. 11 shows the curvatures developed along the four specimens at different stages of loading. The curvatures were computed from displacement transducer measurements as described in Liu (2012). The yield curvatures, ϕ_y, were calculated using the approximate formula $\phi_y = 2.25\varepsilon_y/D$, where D is the diameter of the member and ε_y is the yield strain of the longitudinal reinforcement (Priestley 2003). As shown, the maximum curvatures measured from the bottom 25 to 40% of the columns exceeded the yield curvature. The curvatures developed in the piles were smaller than the yield curvature. Specimens 2 and 3 showed similar curvature variations for the columns, but the pile curvature was not obtained for Specimen

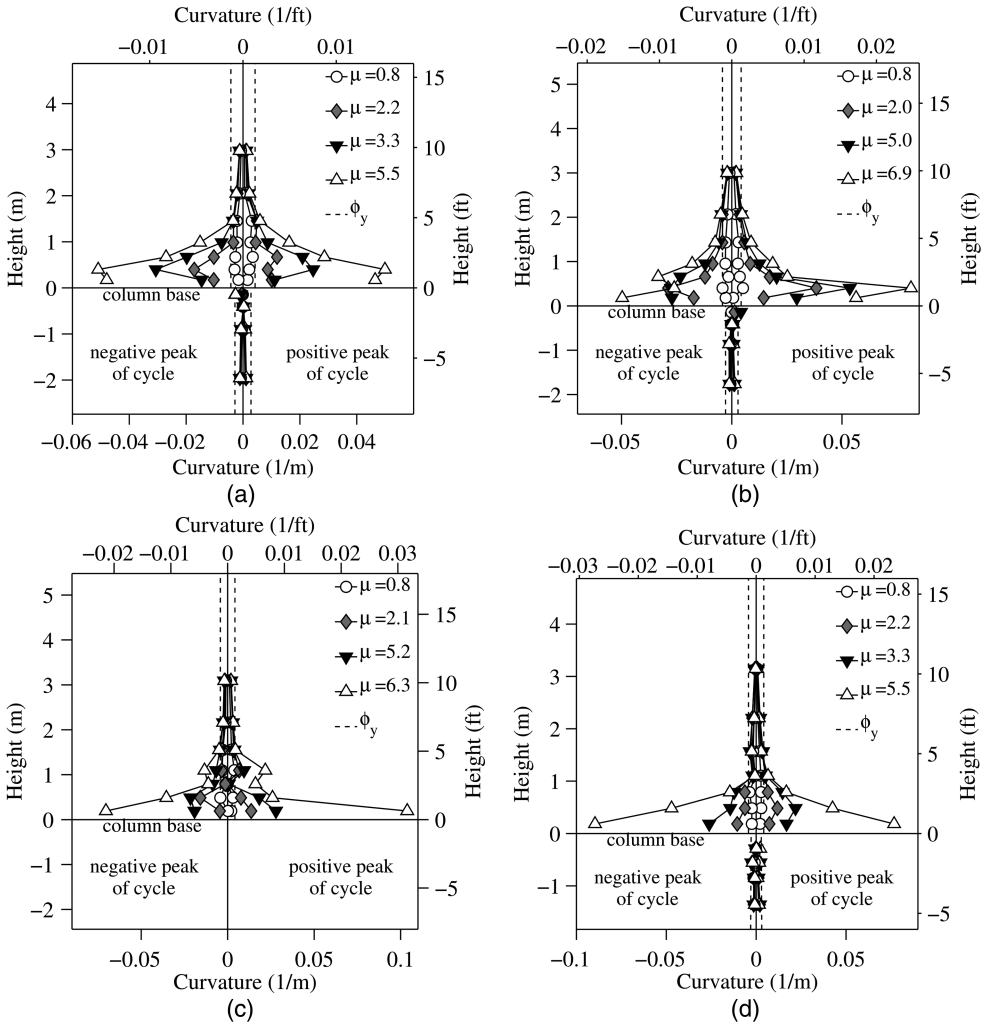

Fig. 11. Curvature distributions: (a) Specimen 1; (b) Specimen 2; (c) Specimen 3; (d) Specimen 4

3, which had a steel casing. The plastic curvature developed in the column of Specimen 3 appears to be more localized at the base of the column as compared to the other specimens. This could be attributed to the more-severe plastic strains developed in the longitudinal bars at the base of the column due to reduced plastic strain penetration into the pile, as discussed in a previous section.

Strains in Reinforcing Bars

Column Longitudinal Reinforcement

For each specimen, strains in two of the column longitudinal bars at the north face and two at the south face were measured, as shown in Fig. 3, along the lower half of the column and the pile segment. The strain values at the peak displacements of different cycles are shown in Fig. 12. Plastic strains developed near the base of the columns and penetrated into the bar anchorage region in the piles. In general, the extent of penetration of plastic strains into the anchorage region of these bars inside the pile depends on the bond between the bar and the surrounding concrete. A weaker bond will result in more-significant bar slip and more-severe plastic strain penetration. The plastic deformation of a bar can significantly reduce the bond strength between the bar and the surrounding concrete (Shima et al. 1987). For Specimen 1, the maximum plastic strain penetration measured in the bars at $\mu = 5.5$ was 610 mm (2 ft), which is 17 times the bar diameter, d_b, or 27% of the embedment length of the column reinforcement. For Specimen 2, the maximum plastic strain penetration measured in the bars at $\mu = 5.0$ was 915 mm (3 ft) or $21d_b$, which represents 50% of the embedment length. Hence, the lower half of the embedment length, which is $21d_b$, was able to develop the yield strength of the bar. According to the development length tests conducted by Murcia-Delso et al. (2015) on individual bars embedded in concrete with similar strengths and confinement levels, a length of $10d_b$ is sufficient to develop the yield strength of a bar in tension. At higher ductility demand levels, all the strain gauges (or more likely the wires) along the embedment length of the column reinforcement in Specimen 2 were damaged. For Specimen 3, most of the strain gauges provided reliable readings until the end of the test, and the maximum plastic strain penetration measured at $\mu = 6.3$ was 610 mm (2 ft) or $14d_b$, which is 33% of the embedment length of the column reinforcement. The reduction of the plastic penetration in Specimen 3, as compared to Specimen 2, can be attributed to the improved bond resistance of the bars as a result of the additional confinement provided by the steel casing. For Specimen 4, the maximum plastic strain penetration measured at $\mu = 5.5$ was 457 mm (1.5 ft) or $18d_b$, which represents 50% of the embedment length of the column reinforcement.

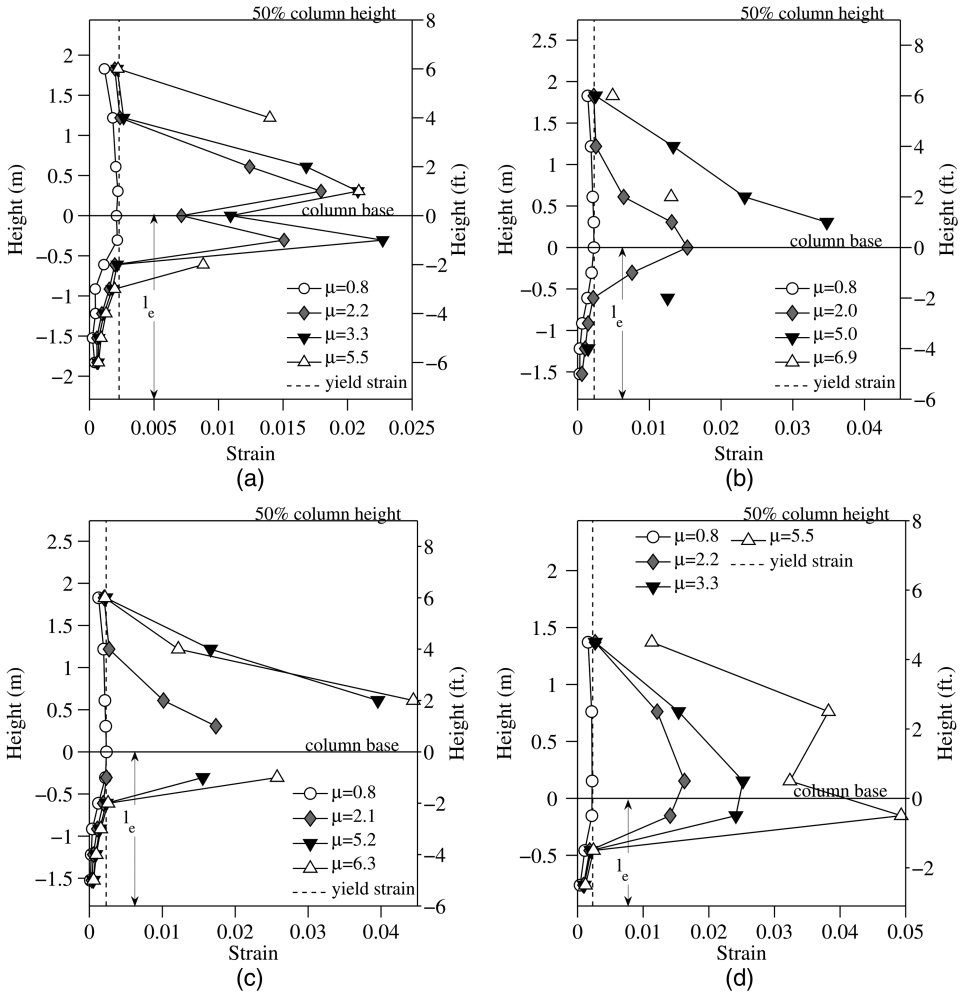

Fig. 12. Tensile strains in column longitudinal reinforcement on the north side of the specimens: (a) Specimen 1; (b) Specimen 2; (c) Specimen 3; (d) Specimen 4

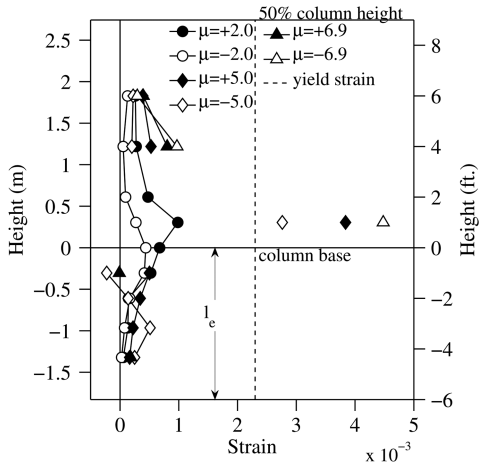

Fig. 13. Hoop strains in the column transverse reinforcement on the south side of Specimen 2

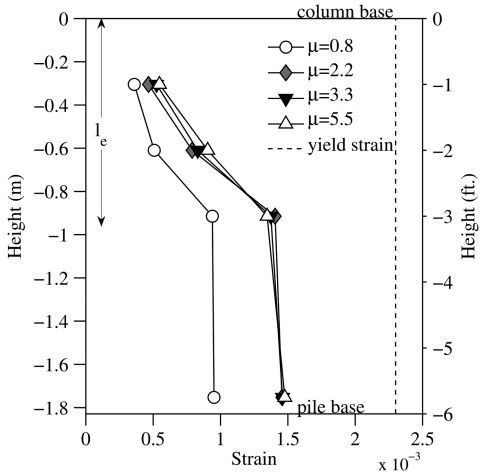

Fig. 14. Tensile strains in pile longitudinal reinforcement on the north side of Specimen 4

Column Transverse Reinforcement

The strains in the transverse hoops of the columns were measured at the north and south faces of the columns, as shown in Fig. 3. Fig. 13 shows the hoop strains measured on the south side of the column in Specimen 2 at the peak displacements of different cycles. The hoops remained elastic, except those located at the base of the columns, which experienced large inelastic deformations caused by the crushing of the core concrete and the buckling of the longitu-

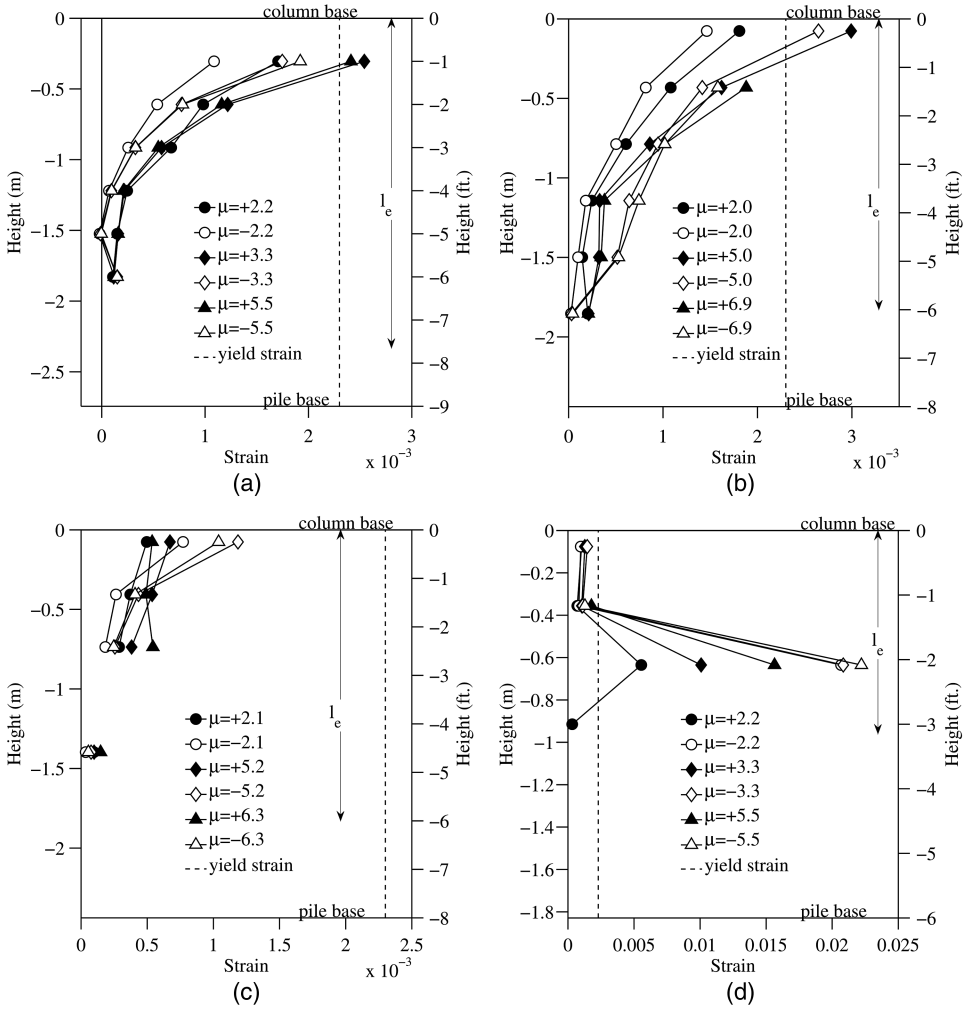

Fig. 15. Hoop strains in the pile transverse reinforcement on the south side of the specimens: (a) Specimen 1; (b) Specimen 2; (c) Specimen 3; (d) Specimen 4

dinal bars. However, none of the hoops fractured. Hoops in the columns of the other specimens behaved similarly. As shown in Fig. 13, the tensile hoop strains measured on the south side near the base of the column were larger when the displacements were positive, i.e., when the concrete and the longitudinal bars on the south side were subjected to compression. A similar trend was observed for the hoop strains measured on the north side of the specimens.

Pile Longitudinal Reinforcement

Fig. 14 shows the tensile strains in the pile longitudinal bar located at the extreme north side of Specimen 4 measured at the maximum southward displacements in different load cycles. The bar remained elastic, and the bar strains in the region where the column longitudinal reinforcement was embedded [0 to 0.94 m (3.1 ft)] varied more or less linearly with distance, indicating a relatively uniform bond stress distribution along the bar. The longitudinal bars in the piles of the other specimens behaved similarly.

Pile Transverse Reinforcement

Fig. 15 presents the strains measured in the exterior hoops in the bar anchorage region of the piles at the peak displacements of different cycles. The strains were measured at the extreme south side of the specimens. Except for Specimen 4, the hoop strains in the upper portion of the piles were larger than those in the lower portion. The hoops located in the lower part of the bar anchorage region experienced practically no strain. The different hoop strains at the

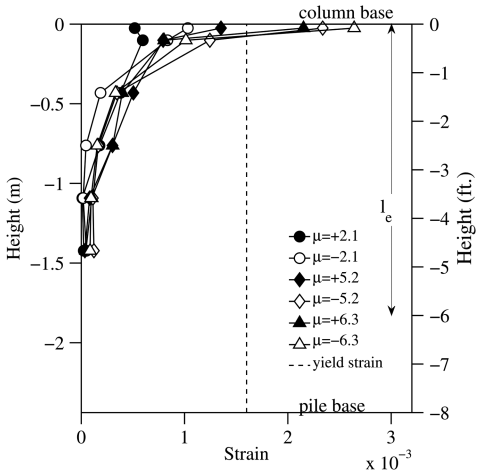

Fig. 16. Hoop strains in the steel casing on the south side of Specimen 3

top and bottom of the bar anchorage region can be partly due to the fact that the longitudinal bars of the columns tended to slip more and thereby exert larger splitting forces in the top region of the piles, and partly to the prying action of the confined column core in the pile. For Specimens 1 and 2, the strains in the pile hoops were in general relatively small and below the yield strain except for the first hoop at the top, which had strains slightly beyond the yield strain. The pile hoops in Specimen 3, which had a steel casing around the pile, did not yield at all. As shown in Fig. 16, the hoop strains in the steel casing are similar to those in the hoops at the same elevations; the strains near the top of the casing were, however, larger and exceeded the yield strain in later cycles.

The hoop strains measured in Specimen 4 are in general higher than those in the other specimens, which could be attributed to the smaller diameter of the pile as compared to the other specimens. The smaller pile diameter resulted in a thinner concrete ring to resist the splitting forces induced by slip of the column bars and the prying action exerted by the confined core of the column. This is consistent with the observation that the vertical splitting cracks in the pile of Specimen 4 were more severe and wider than those in the other specimens. The largest strain was measured in the hoop located at 0.64 m (2.1 ft) from the base of the column, and it was 0.022 (or approximately 10 times the yield strain); however, no other hoops yielded. The reason for the maximum hoop strain occurring near the bottom part of the bar anchorage region and not at the top is unclear, but it could be related to the severe prying action of the column in this region.

Conclusions

Four full-scale column–pile assemblies were constructed and subjected to quasi-static cyclic lateral loading to investigate the possibility of reducing the embedment length for column longitudinal reinforcement extending into oversized pile shafts, as compared to that required by current design specifications. Specimen 1 had an embedment length of $D_{c,\max} + l_d$, which was close to the minimum requirement of Caltrans (2013) and AASHTO (2011). Specimens 2 through 4 had embedment lengths reduced to $l_d + s + c$. Despite the difference in the embedment lengths, all specimens showed a ductile behavior. The columns developed a plastic hinge at the base and failed by the buckling and subsequent fracture of one or more longitudinal bars in the plastic-hinge region. Damage in the piles was limited to cone-shaped cracks and tensile splitting cracks near the base of the column. Specimen 3 had very light damage in the pile owing to the increased confinement provided by an engineered steel casing.

The maximum penetration distance of plastic tensile strains measured in the column longitudinal bars into the piles was between 14 and $21d_b$. Specimens 2 and 4, which had an embedment length of $l_d + s + c$, had the most significant plastic strain penetration. Specimen 2 had the lowest amount of transverse reinforcement in the pile for the given development length, while Specimen 4 had a smaller pile diameter, which could have lowered the confinement effect and thus increased the plastic strain penetration length. Specimen 3 had the lowest plastic strain penetration. This can be attributed to the steel casing, which provided a better confinement resulting in better bond resistance.

The test results shown herein indicate that an embedment length of $l_d + s + c$ is sufficient to develop the tensile strength of longitudinal reinforcement in bridge columns extending into oversized pile shafts. Adequate transverse reinforcement must be provided in the bar anchorage region of a pile shaft to control tensile splitting cracks. Eqs. (4) and (5) proposed in this study can be used to determine the transverse reinforcement required as proven by the test results. An engineered steel casing designed with Eq. (5) can effectively arrest tensile splitting cracks in a pile shaft. A better confinement provided by a steel casing may, however, reduce plastic strain penetration in the bar anchorage region and thereby reduce bar slip, resulting in a slightly earlier fracture of the longitudinal bars in the plastic hinge region of the column. In any respect, this influence is very small and bar fracture normally occurs at very large column drift levels. Hence, the benefit of a steel casing far exceeds this small negative influence.

Appendix. Transverse Reinforcement Required for Pile Shafts

The analytical model presented herein assumes that a bar being developed exerts a uniform radial stress, σ, on the surrounding concrete as a result of the wedging action of the bar ribs during slip. For a unit length of the bar, the resultant radial stress can be represented by a set of four splitting forces (Cairns and Jones 1996), $f = \sigma d_b$. Fig. 17 shows the splitting forces induced by the column and pile longitudinal bars in a pile cross section. For simplicity, it is assumed that all the column bars are subjected to tension. In reality, some could be in compression, but the bars in compression will also induce splitting forces as they slip.

Assuming that the magnitude of the radial stress σ is equal to the bond stress, τ, as suggested by Tepfers (1973), the splitting force per unit length of the bar can be expressed as $f = |\tau_{\text{col}}| d_{b,\text{col}}$ for the column bars and $f' = |\tau_{sh}| d_{b,sh}$ for the bars in the pile. Since the forces from the column longitudinal bars have to be transferred to the pile longitudinal bars, the total bond force per unit length of the column bars has to be equal to that of the pile bars over the bar anchorage region. Hence

$$N_{\text{col}} |\tau_{\text{col}}| d_{b,\text{col}} = N_{sh} |\tau_{sh}| d_{b,sh} \tag{6}$$

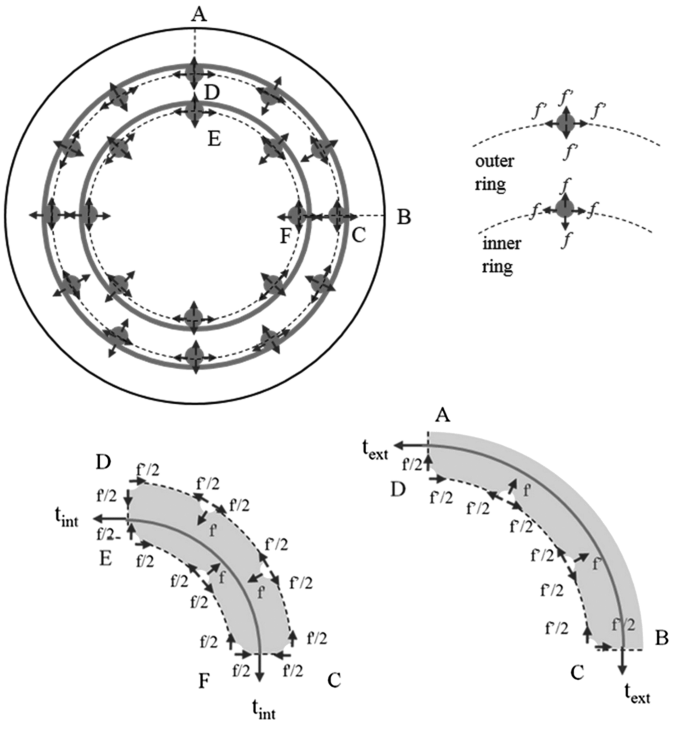

Fig. 17. Splitting forces in pile shaft

in which N_{col} = total number of bars in the column and N_{sh} = number of bars in the pile shaft. By substituting $f' = |\tau_{sh}|d_{b,sh}$ into Eq. (6), the value of f' can be obtained as shown in Eq. (7)

$$f' = \frac{N_{col}}{N_{sh}}|\tau_{col}|d_{b,col} \tag{7}$$

Next, equilibrium is considered for the free bodies ABCD and CDEF shown in Fig. 17. The forces acting on the two free bodies are the splitting forces of the bars, f and f', and the tensile forces, t_{ext} and t_{int}, in the outer (pile) and inner (column) horizontal hoops. Line AB is a free surface with no forces, and it is assumed that the concrete is split along lines AD, DC, CB, DE, EF, and FC. Therefore, the concrete does not transfer any forces along these lines. For the free body ABCD, the splitting forces in the tangential direction can be ignored because these forces cancel each other. The splitting forces pointing in the radial direction exert a uniform pressure, p_{ext}, which can be calculated from f' as follows:

$$p_{ext} = \frac{N_{sh}f'}{\pi D_{ext}} = \frac{N_{col}|\tau_{col}|d_{b,col}}{\pi D_{ext}} \tag{8}$$

in which D_{ext} = diameter of the outer reinforcing hoops. Based on the equilibrium of the free body ABCD, the tensile force, t_{ext}, to be provided by the hoops in a unit length of the pile to balance p_{ext} is

$$t_{ext} = p_{ext}\frac{D_{ext}}{2} = \frac{N_{col}|\tau_{col}|d_{b,col}}{2\pi} \tag{9}$$

In the free body CDEF, the splitting forces in the tangential direction can be ignored based on the same argument presented for ABCD. Based on the equilibrium of the free body CDEF, the tensile force, t_{int}, to be provided by the inner hoops to balance for the difference in pressures p_{ext} and p_{int}, generated by the radial splitting forces exerted by the longitudinal bars, is

$$t_{int} = p_{int}\frac{D_{int}}{2} - p_{ext}\frac{D_{ext}}{2} \tag{10}$$

in which D_{int} = diameter of the inner (column) reinforcing hoops. The internal pressure, p_{int}, generated by the slip of the column bars, is given by

$$p_{int} = \frac{N_{col}f'}{\pi D_{int}} = \frac{N_{col}|\tau_{col}|d_{b,col}}{\pi D_{ext}} \tag{11}$$

Substituting Eqs. (8) and (11) in Eq. (10) results in the condition that $t_{int} = 0$. Hence, the inner hoops will not develop tension and can be considered ineffective for resisting the splitting forces.

Sufficient transverse reinforcement has to be provided in the pile to develop the tensile force t_{ext}, and the amount is given by Eq. (12)

$$t_{ext} = \frac{A_{tr}}{s_{tr}}f_{y,tr} \tag{12}$$

in which s_{tr} = spacing; A_{tr} = cross-sectional area; and $f_{y,tr}$ = nominal yield stress of the transverse hoops or spiral. In reality, the bond-stress distribution along the development length of a bar is not uniform and the location of the peak stress depends on the extent of the plastic strain penetration (Murcia-Delso et al. 2013a, 2015). A conservative approach to determine the amount of transverse steel required is to consider only the peak bond stress and assume that its value is equal to the maximum bond strength, τ_{max}. The peak bond stress will actually be lower than τ_{max} due to the tensile yielding of the bars. Substituting τ_{col} with τ_{max} and combining Eqs. (9) and (12) results in Eq. (13), which determines the amount of transverse hoops required to prevent bar anchorage failure due to concrete splitting

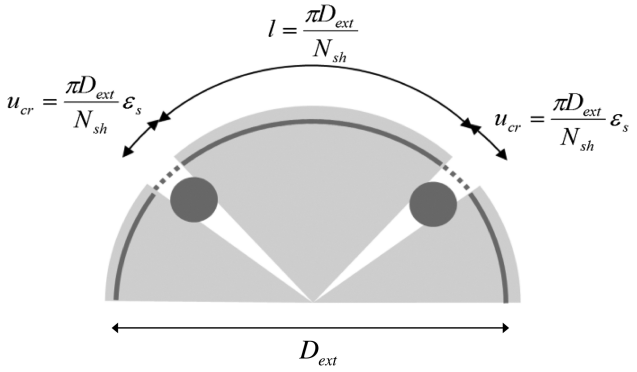

Fig. 18. Splitting crack opening and strain in hoop reinforcement

$$A_{tr} = \frac{1}{2\pi}\frac{N_{col}\tau_{max}d_{b,col}s_{tr}}{f_{y,tr}} \tag{13}$$

Given the uncertainty in the location of the peak bond stress, the transverse steel calculated with Eq. (13) should be provided along the entire bar anchorage region.

To control the width of the splitting cracks induced by bar slip, more transverse reinforcement than what is calculated with Eq. (13) is needed. To calculate this amount, an assumption is made that a radial splitting crack develops along every longitudinal bar of the pile as the bars slip, which was observed in the column-pile tests. The opening of a splitting crack will induce strain in the transverse reinforcement. Assuming that the strain in a transverse reinforcing hoop is uniform and that all the cracks have the same widths, Eq. (14) provides the relation between the strain in the transverse hoops, ε_s, and the width of a radial crack, u_{cr}, as illustrated in Fig. 18

$$u_{cr} = \frac{\pi D_{ext}}{N_{sh}}\varepsilon_s \tag{14}$$

The maximum allowable strain, $\varepsilon_{s,max}$, in the transverse hoops is then related to the maximum allowable crack width $u_{cr,max}$ as follows:

$$\varepsilon_{s,max} = \frac{u_{cr,max}N_{sh}}{\pi D_{ext}} \tag{15}$$

For the purpose of controlling the crack width, the transverse hoops have to remain elastic, i.e., $\varepsilon_{s,max} < \varepsilon_y$. Hence, the amount of transverse reinforcement required can be determined by replacing $f_{y,tr}$ in Eq. (13) with $\varepsilon_{s,max}f_{y,tr}/\varepsilon_y$, which results in Eq. (16*a*)

$$A_{tr} = \frac{1}{2\pi}\frac{N_{col}\tau_{max}d_{b,col}s_{tr}}{\alpha f_{y,tr}} \tag{16a}$$

where

$$\alpha = \frac{\varepsilon_{s,max}}{\varepsilon_y} = \frac{u_{cr,max}N_{sh}}{\pi D_{ext}\varepsilon_y} \le 1 \tag{16b}$$

When an additional steel casing is to be provided around the pile, formulas to determine the required thickness of the steel casing, t_c, can be derived in a similar way by replacing Eq. (12) with the following equation

$$t_{ext} = \frac{A_{tr}}{s_{tr}}f_{y,tr} + t_c f_{y,c} \tag{17}$$

in which $f_{y,c}$ = yield strength of the casing steel.

Acknowledgments

Funding for the research presented in this paper was provided by Caltrans under Contract No. 59A0710. The authors appreciate the technical input provided by Caltrans engineers throughout this study. However, the opinions expressed in this paper are those of the authors and do not necessarily reflect those of the sponsor. The experiments presented in this paper were conducted in the Charles Lee Powell Structural Engineering Laboratories at UC San Diego. The authors would like to express their gratitude to the laboratory staff for their professionalism and high-quality technical support. The authors would also like to thank Mr. Charles Cummings, a former UC San Diego undergraduate student, for his assistance in the preparation of the column–pile assembly tests.

References

AASHTO. (2010). *LRFD bridge design specifications*, 5th Ed., Washington, DC.

AASHTO. (2011). *AASHTO LRFD seismic bridge design specifications*, 2nd Ed., Washington, DC.

AASHTO. (2012). *LRFD bridge design specifications*, 6th Ed., Washington, DC.

ACI (American Concrete Institute). (2001). "Control of cracking of concrete structure." *ACI 224R-01*, Farmington Hills, MI.

ASTM. (2009). "Standard specification for low-alloy steel deformed and plain bars for concrete reinforcement." *ASTM A706/A706M-09b*, West Conshohocken, PA.

Cairns, J., and Jones, K. (1996). "An evaluation of the bond-splitting action of ribbed bars." *ACI Mater. J.*, 93(1), 10–19.

Caltrans (California Department of Transportation). (2008). "Bridge design specifications." Sacramento, CA.

Caltrans (California Department of Transportation). (2013). "Caltrans seismic design criteria, version 1.7." Sacramento, CA.

Liu, Y. (2012). "Lateral behavior of reinforced concrete columns supported on type II shafts." M.S. thesis, Dept. of Structural Engineering, Univ. of California, San Diego.

Lukose, K., Gergely, P., and White, R. N. (1982). "Behavior of reinforced concrete lapped splices for inelastic cyclic loading." *ACI J.*, 79(5), 355–365.

McLean, D. I., and Smith, C. L. (1997). "Noncontact lap splice in bridge column-shaft connections." *Rep. No. WA-RD 417.1*, Washington State Transportation Center, Washington State Univ., Pullman, WA.

Murcia-Delso, J., Shing, P. B., Stavridis, A., and Liu, Y. (2013a). "Required embedment length of column reinforcement extended into type II shafts." *Rep. No. SSRP–13/05*, Dept. of Structural Engineering, Univ. of California, San Diego.

Murcia-Delso, J., Stavridis, A., and Shing, P. B. (2013b). "Bond strength and cyclic bond deterioration of large-diameter bars." *ACI Struct. J.*, 110(4), 659–670.

Murcia-Delso, J., Stavridis, A., and Shing, P. B. (2015). "Tension development length of large-diameter bars for severe cyclic loading." *ACI Struct. J.*, 112(6), 689–700.

Priestley, M. J. N. (2003). *Myths and fallacies in earthquake engineering, revisited*, IUSS Press, Pavia, Italy.

Sagan, V. E., Gergely, P., and White, R. N. (1991). "Behavior and design of noncontact lap splices subjected to repeated inelastic tensile loading." *ACI Struct. J.*, 88(4), 420–431.

Shima, H., Chou, L., and Okamura, H. (1987). "Bond characteristics in post-yield range of deformed bars." *Proc. JSCE*, 6(378), 113–124.

Tepfers, R. (1973). *A theory of bond applied to overlapped tensile reinforcement splices for deformed bar*, Division of Concrete Structures, Chalmers Univ. of Technology, Goteborg, Sweden.

Tran, H. V., Stanton, J. F., and Eberhard, M. O. (2013). *Precast bent system for high seismic regions: Laboratory tests of column-to-drilled shaft socket connections*, Federal Highway Administration.